DOI: 10.1002/stco.70013

Felix Eyben, Helen Bartsch, Markus Feldmann

ARTICLE

Fitting of mechanical material behaviour of structural steel for numerical modelling

Development of an optimization algorithm

Numerical simulations are widely used in structural engineering research, and validated models enable the efficient expansion of datasets without costly additional testing. They allow the investigation of alternative geometries and loading scenarios beyond those covered by experiments. Their reliability, however, depends strongly on the accuracy of the material modelling. In structural steel, elastic behaviour is well captured by Hooke's law, but the plastic range remains challenging to describe realistically. Existing hardening models provide mathematical representations of the plastic portion of the true stress–strain curve, yet numerous studies have shown that these models require extensive calibration to reproduce experimental behaviour satisfactorily. This calibration is typically iterative, time-consuming, and often yields results that still offer potential for refinement. To address this, an automated optimization tool has been developed to fit flow curves directly from uniaxial tensile test data. This article outlines the fundamentals of material modelling for steel in numerical simulations and presents the development and validation of the proposed optimization algorithm, which allows realistic numerical modelling on a scientific level and aligns with the ongoing standardization efforts in prEN 1993-1-14.

Keywords structural steel; numerical simulations; material characterization; finite-element simulations; plasticity; optimization

1 Introduction

Nowadays, in steel construction research, numerical simulations performed by finite-element models (FEMs) have become common practice, e.g., for examining complex details where analytical approaches are of limited use. To answer research questions or develop design guidelines, expensive experiments are required. Thus, not all necessary investigations can be conducted experimentally. Therefore, numerical simulations are employed to extend the dataset. Typically, these simulations are validated against experimental results first to ensure their accuracy in representing reality. The accuracy of the simulations heavily depends on the definition of material properties.

A lot of internationally published and own conducted research projects have shown the potential of numerical simulations that calculate plastic component behaviour. In [1, 2], for example, numerical simulations were used to recalculate experimental three-point-bending tests on high-strength steel beams. With the calibrated FEMs, extensive parametric studies were conducted to show the general ability of high-strength steels to form a sufficient rotational capacity for a plastic design. Based on the experimental results in combination with the numerical results, design recommendations could be derived. The power of numerical simulations calculating plastic component behaviour was also shown in [3], where simulations were used to investigate the burst behaviour of pressure vessels, or [4], where high-strength steels were in focus. Also, the correct simulation of plastic material behaviour due to large cyclic hysteresis has been shown [5]. The huge number of validations of numerical simulations has also prompted their inclusion in standardization efforts. In the current revision of the relevant European standard, a new part, prEN 1993-1-14 [6], will specifically address the design assisted by FE simulations. To simulate the material behaviour of steel, elastic and plastic properties must be incorporated into the simulation models. While elastic parameters are well defined, establishing appropriate plastic properties, expressed as flow curves to model the non-linear material behaviour, presents challenges. Various hardening models, such as the Hollomon [7] or Ludwik [8] model, the Ramberg–Osgood [9] relationship, or other bilinear or multilinear models, such as those in prEN 1993-1-14 [6], can be used based on standard material characteristics, e.g., yield or tensile strength. Nonetheless, numerous research activities, [1, 3, 10], have demonstrated the necessity of calibrating these hardening models, e.g., based on round bar tensile tests, for accurate simulation, often requiring time-consuming calibration processes.

An automated optimization tool was developed to improve the results and at the same time reduce the effort required for the calibration of flow curves. In the following, the basic principles on the material behaviour of steel,

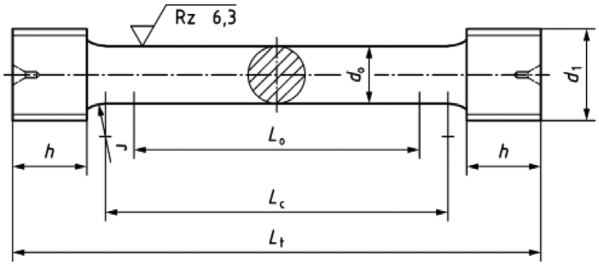

Fig. 1 Tensile specimen form B: round specimen with threaded heads [12]

its definition for numerical simulations, the general procedure to derive flow curves, the developed algorithm, and its validation on three exemplary steels will be presented. For the validation, laboratory and component scale is considered.

2 State of art: Material behaviour of steel and definition for numerical investigations

2.1 Material behaviour of structural steel under uniaxial tension

Typically, the stress–strain behaviour of a material is extracted from uniaxial tensile tests. The most common standard on tensile tests used in Germany industry is the DIN ISO 6892-1 [11], which specifies the method for tensile testing of metallic materials and defines the mechanical properties which can be determined at room temperature. The standard DIN 50125 [12] defines the geometry of metallic specimens. In Fig. 1, a tensile specimen of form B, round bar, is indicated.

As a result, the engineering stress–strain relation can be extracted using the following equations for calculating the engineering stress (σ_{eng}) and engineering strain (ε_{eng}) in dependence of the initial specimen geometry. Here, the load F, applied in direction of specimen length axis, is measured in the test as well as the current gauge length L. For calculating the engineering stress–strain curve, the parameters are related to the initial specimen geometry, resp. L_0 as initial gauge length and A_0 as initial cross-section area.

$$\sigma_{\text{eng}} = \frac{F}{A_0} \tag{1}$$

$$\varepsilon_{\text{eng}} = \frac{\Delta L}{L_0} = \frac{L - L_0}{L_0} \tag{2}$$

Typical engineering stress–strain curves are indicated in Fig. 2 for a mild steel with (left) and a high-strength steel without a yield plateau (right).

The material behaviour must be interpreted with caution beyond the elastic limit since the specimen experiences a change from its original parameters [14]. In order to predict the true behaviour, it is more meaningful to plot the data in terms of the true stress (σ_{true}) and true strain ($\varepsilon_{\text{true}}$), where stress and strain are related to the current cross-sectional area (A) and current length (L) values of the specimen during deformation:

$$\varepsilon_{\text{true}} = \ln\left(\frac{L}{L_0}\right) \tag{3}$$

$$\sigma_{\text{true}} = \frac{F}{A} \tag{4}$$

At very low strains, the differences between true and engineering stress–strain curves are very small. Thus, it is irrelevant whether Young's modulus is defined in terms of engineering or true stress strain [15].

In the region with uniform deformation after yielding, the material flows with negligible change in volume [14]. Therefore, the assumption of volume constancy can be considered and is described as

$$A_0 \cdot L_0 = A \cdot L \tag{5}$$

Then true and engineering stresses as well as strains can be related to each other according to Eq. (6) and Eq. (7):

$$\sigma_{\text{true}} = \sigma_{\text{eng}} \cdot (1 + \varepsilon_{\text{eng}}) \tag{6}$$

$$\varepsilon_{\text{true}} = \ln(1 + \varepsilon_{\text{eng}}) \tag{7}$$

The previous relationships described in Eq. (6) and Eq. (7) are valid until the point where necking begins. As an example, Fig. 3 indicates a comparison of an engineering and true stress–strain curve and also the point, where necking begins.

Beyond the maximum load point, the true stress is still valid to Eq. (6) and the true strain should be determined based on the current area of the specimen as:

$$\varepsilon_{\text{true}} = \ln\left(\frac{A_0}{A}\right) \tag{8}$$

2.2 Material formulation for FE simulations

To implement the material behaviour of steel, e.g., into FEM simulations, the behaviour of steel gets split into the elastic and plastic components.

The elastic behaviour is well described by the Hooke's law (Eq. (9)) and is defined as a linear relationship between

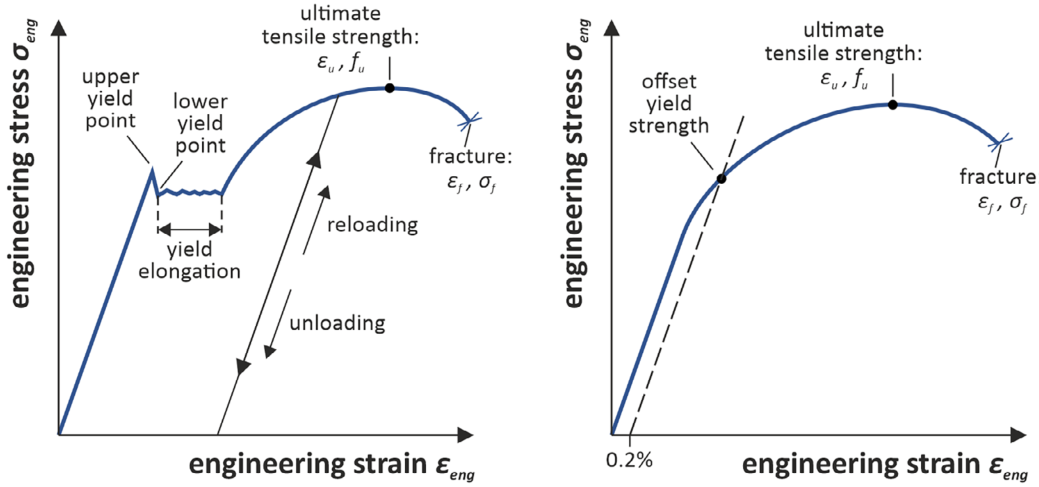

Fig. 2 Engineering stress–strain curves for steel with (left) and without (right) yield plateau [13]

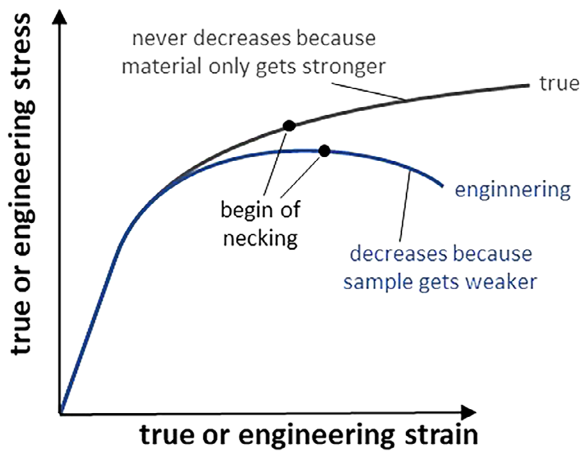

Fig. 3 Comparison of engineering and true stress–strain curves for steel [16]

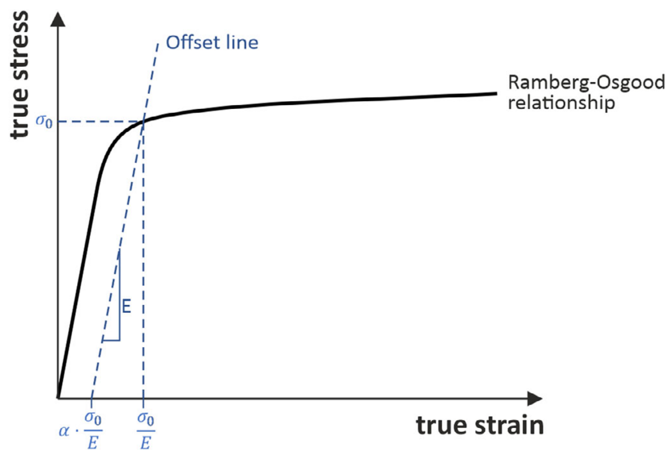

Fig. 4 Ramberg–Osgood relationship [9]

strain ε and stress σ. The Young's modulus E defines the slope.

$$\sigma = E \cdot \varepsilon \tag{9}$$

The elastic deformation is the reversible deformation of a component subjected to external forces. With the increase of the external load, the same component can experience inelastic or permanent deformation, which is known as plastic deformation. At the point, where the yield strength f_y of the steel is reached, the plastic behaviour begins.

The plasticity theory is concerned with the mathematical study of stress and strain in plastically deformed solids with particular reference to metals [17], and it dates back to 1864 when Tresca identified the behaviour of several materials in his experimental results. Since then, further development to establish the laws of plasticity was made by Saint-Venant, Levy, Haar and von Karman, von Mises, Hencky, Prandt, Prager, Hill, and Drucker, among others [17]. The stress–strain relationship of structural steel is often described by the Ramberg–Osgood relationship [9], which is also implemented in prEN 1993-1-14 [6].

The Ramberg–Osgood relationship, Fig. 4, is a phenomenological model to describe the non-linear stress–strain relationship for steels without a yield plateau [9]. The model includes also the elastic part.

The Ramberg–Osgood equation is

$$\varepsilon = \frac{\sigma}{E} + \alpha \cdot \frac{\sigma_0}{E} \left(\frac{\sigma}{\sigma_0} \right) \tag{10}$$

with ε = true strain, σ = true stress, E = Young's modulus, σ_0 = initial yield stress, α = constant whereby the yield offset is defined as follows:

$$\alpha \cdot \frac{\sigma_0}{E} = 0.002 \tag{11}$$

But for numerical simulations, the flow curve is a necessary input parameter. It is defined as only the plastic part

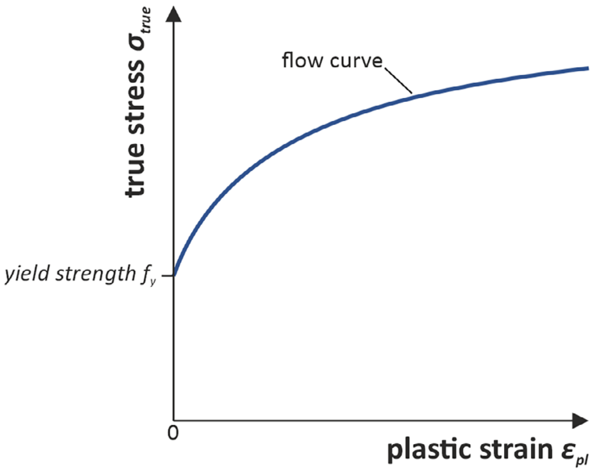

Fig. 5 Typical flow curve for a constant strain rate and temperature

of the true stress–strain relation and starts at 0% plastic strain $\varepsilon_{\mathrm{pl}}$.

2.2.1 Definition: Flow curve

The flow stress is the stress that causes plastic deformation in a uniaxial stress state and it depends on the material, strain, strain rate, and temperature [18]. For the specific case of a tensile test, the plastic part of the true stress–strain curve that represents the true stress σ_{true} variation with the plastic true strain $\varepsilon_{\mathrm{pl}}$, strain rate $\dot{\varepsilon}$, and temperature T is also known as the flow curve. Fig. 5 shows a typical flow curve.

This concept is associated with plasticity theory and hardening models, such as isotropic and kinematic hardening. For the case of isotropic hardening, the expansion (or contraction) of the yield locus is expressed by the flow curve. As the material deforms, the hardening level on the flow curve moves forward with the accumulated plastic strains, and as a result the yield locus expands isotopically in all directions, as shown in Fig. 6 [19].

The concept of flow curve is industrially well accepted in the processes that involve large plastic deformations, such as metal forming, where it is considered as necessary for the prediction of forming forces, tool deflection, and material flow [20]. The description of the flow curve in the strain hardening regions is frequently done by mathematical models [21], physical models [22], or also known as power laws [23]. The most common hardening models to define a flow curve for structural steel are Hollomon, Ludwik, Swift, and Voce, which are given in the following. All hardening models define a true stress σ_{true} in dependence of the plastic strain $\varepsilon_{\mathrm{pl}}$ to describe flow curves, as shown in Fig. 5.

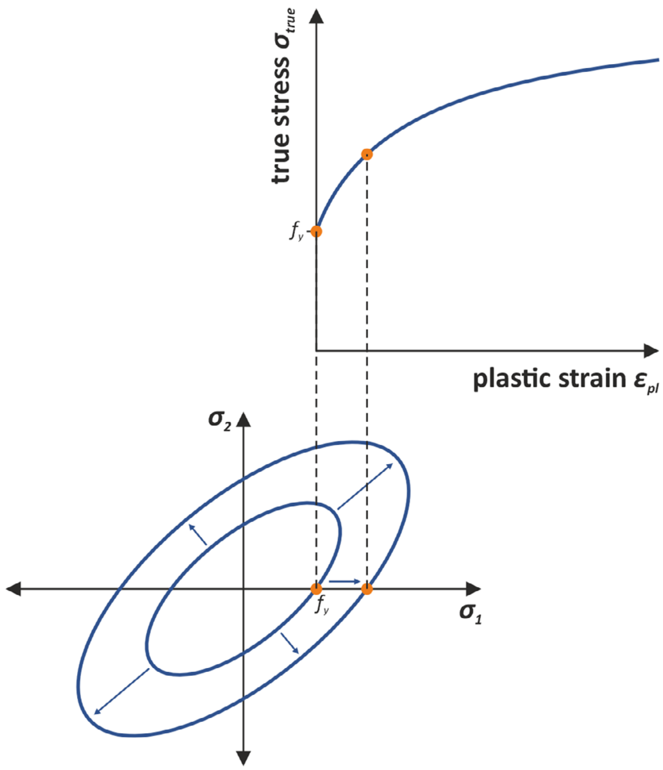

Fig. 6 Isotropic expansion of the yield locus as a function of hardening [19]

2.2.2 Hollomon Model [7]

The Hollomon model is commonly used to represent the material true stress–strain behaviour of metallic materials, such as steel, copper, and alloys [7]:

$$\sigma = k_{\mathrm{H}} \left(\varepsilon_{\mathrm{pl}}\right)^{n_{\mathrm{H}}} \tag{12}$$

with: k_{H} = strength coefficient, ε_{p} = true plastic strain, and n_{H} = hardening exponent.

2.2.3 Ludwik model [8]

Another well-known empirical description of the flow stress is done by the Ludwik model [8]:

$$\sigma = \sigma_0 + k_{\mathrm{L}}\left(\varepsilon_{\mathrm{pl}}\right)^{n_{\mathrm{L}}} \tag{13}$$

with: σ_0 = yield strength, k_{L} = strength coefficient, and n_{L} = hardening exponent.

As can be seen from Eq. (12) and Eq. (13), the Ludwik model only differs from the Hollomon model by an additional term of σ_0. For the case of materials with a yield plateau, the Ludwik equation is adjusted to consider the length of the yield plateau:

$$\sigma = \sigma_0 + k_{\mathrm{L}}\left(\varepsilon_{\mathrm{pl}} - \varepsilon_{\mathrm{p,eL}}\right)^{n_{\mathrm{L}}} \tag{14}$$

with: $\varepsilon_{\mathrm{p,eL}}$ = true plastic strain at lower yield strain.

2.2.4 Swift model [24]

The shape of the Swift model is similar to the description done by Hollomon. In this case, the stress is shifted along a positive strain axis through a distance equal to the initial strain ε_0. This makes the Swift model more appropriate in the use of processes where a prestrain effect is present, such as cold forming. The Swift model is represented by the following equation:

$$\sigma = k_S \left(\varepsilon_{pl} - \varepsilon_0\right)^{n_S} \tag{15}$$

with: k_S = strength coefficient, ε_0 = initial strain, and n_S = hardening exponent.

2.2.5 Voce model [25]

The Voce model is used for materials where the flow stress shows non-linearity with the increment of the plastic strain first, which saturates into a constant value. In this case, the model is defined as follows:

$$\sigma = \sigma_{sat} + (\sigma_0 - \sigma_{sat}) \cdot \exp\left(-\varepsilon_{pl}/\varepsilon_0\right) \tag{16}$$

with: σ_{sat} = saturation stress, σ_0 = initial yield stress, and ε_0 = characteristic strain.

For Ludwik and Hollomon models, the initial values for the coefficients and parameters can be calculated based on the results of the tensile tests. For Swift and Voce models, the initial values are based on the literature or manually defined via a visual comparison.

3 General procedure to determine flow curves based on experimental small-scale tests

Fig. 7 illustrates a simplified flow chart of the general procedure for deriving flow curves manually. In general, the fitting is a phenomenological approach.

The input in the process is the test report according to DIN ISO 6892-1 [11], where the main mechanical properties and engineering stress–strain curve are described. The data are processed and then, by a manual iterative process, the hardening model considered as the 'best fit' is determined through an inverse method via FE simulations. The foundation for fitting flow curves based on the results of uniaxial tensile tests is the hardening models from Section 2, where, in a first step, an initial calibration is done manually based on the mechanical properties.

The tensile test is then simulated with FEM, Fig. 8, using the initially calibrated flow curve. After the simulation, the engineering stress–strain curve can be derived from the FE result. This curve is compared hand-operated

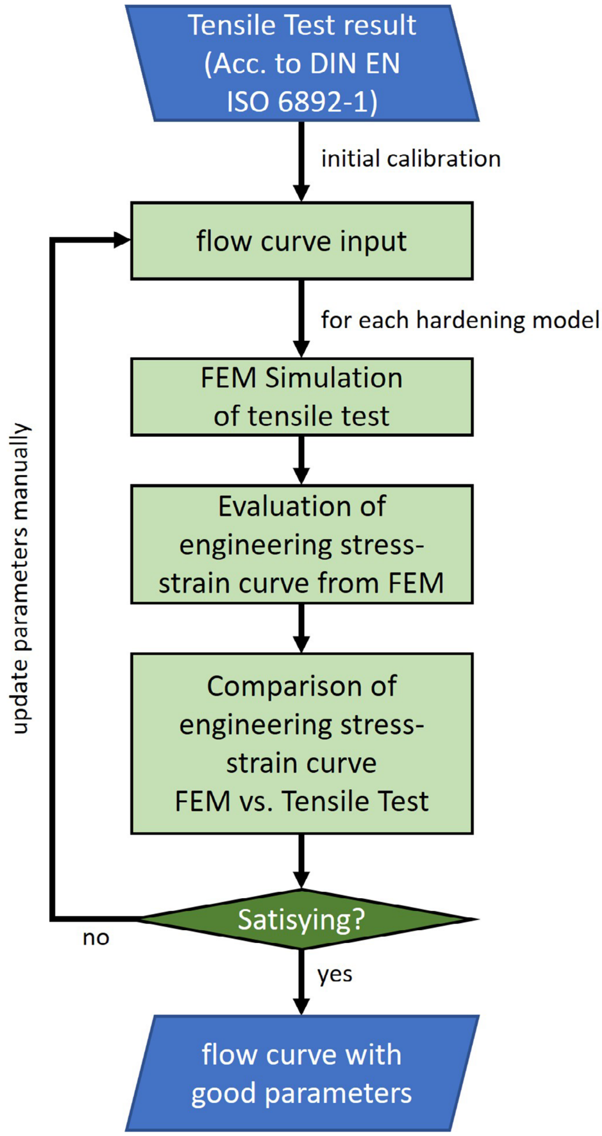

Fig. 7 Simplified flow chart of manual flow curve fitting

to the experimental engineering stress–strain curve and if the match is not satisfying, the flow curve parameters will be updated manually. This is an iterative process until the match between engineering and numerical stress–strain curve is satisfying. The procedure represents a phenomenological approach. The iteration process takes a lot of manual interaction and time to do several iterations for different flow curve parameters.

3.1 The FEM

In the following, the FEM, as modelled in the FE software Abaqus, is presented. The specimen was modelled as a three-dimensional axisymmetric deformable part in the range of the original gauge length. The geometry is based on the specimen type used in the experimental test. In this case, the typically B8x40 (d_0 = 8 mm, L_0 = 40 mm)

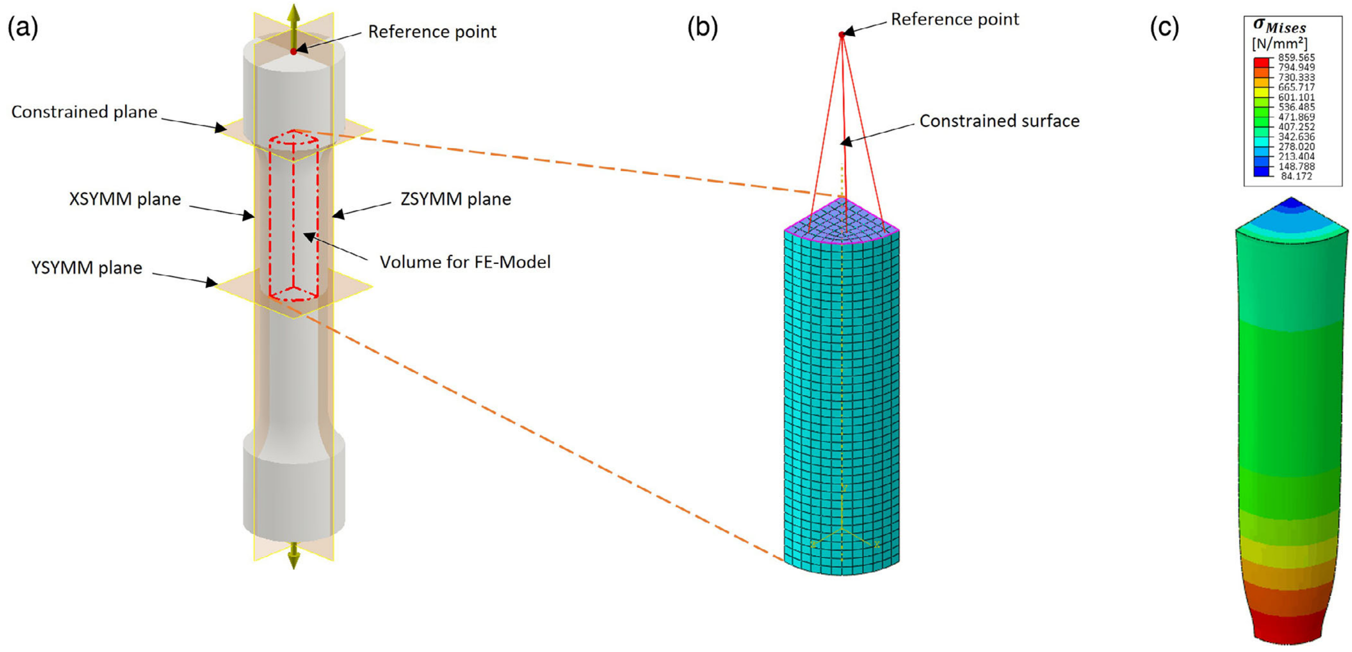

Fig. 8 a) Reference specimen, b) FEM using symmetry, and c) deformed FEM

specimen for round tensile tests is considered. To save computational costs and time, the volume of analysis is defined with symmetry planes. The load, which is always displacement driven to provoke necking, is applied in the length axis of the specimen at a reference point, which is coupled to a constrained plane. Specimen (a), FEM (b), and deformed FEM (c) are shown in Fig. 8.

A mesh with hexahedral elements C3D8R with a mesh size of 0.5 mm for a B8x40 is used. The hardening models are defined in Abaqus by a user subroutine, which is used to define the yield surface size and hardening parameters for isotropic plasticity or combined hardening models.

4 Development of an automatized optimization tool to fit flow curves

4.1 Assumptions

4.1.1 Nominal Young's modulus

The elastic behaviour is described as a linear function with a slope which represents the Young's modulus, Fig. 9. A nominal Young's modulus of $E_{\mathrm{nom}} = 210{,}000\ \mathrm{N/mm^2}$ was assumed.

4.1.2 Flat yield plateau

If the material has a yield plateau, this could also be implemented to the hardening models used. Here, the yield plateau was idealized as flat in the engineering stress–strain curve (on the level of the yield strength f_y between ε_y and ε_n), Fig. 9. However, in numerical models, the material description requires to assign one stress value only once to one strain value. This is why in the definition of the flow curve, a linear segment defined by the yield strength with a very small gradient over the length of the yield plateau is added.

4.1.3 Continuity behaviour at strain hardening point

The hardening model, implemented in a user subroutine, has to be continuous with a constant positive slope.

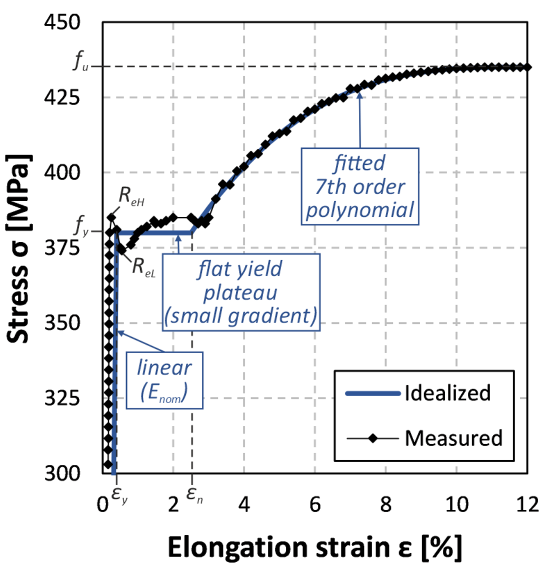

Fig. 9 Sample measured stress–strain curve and the assumed idealization [26]

For the materials that exhibit a yield plateau, the flow curve is defined by two parts. The first one describes the yield plateau behaviour, with the assumption of an ideal flat yield plateau. The second part defines the strain hardening, which can be defined using a polynomial function.

The point, where the flow curve switches from yield plateau to strain hardening, is calculated in the developed subroutine, so that a continuous definition of the flow curve is ensured.

4.2 Optimization methods

4.2.1 General overview

In the developed algorithm, a data matching is to be performed. Data matching means in this case to compare the result of the predicted models (FEM with a specific flow curve) with the actual empirical data (tensile test). There are various ways to measure the 'error' in statistics, a term for the difference between the 'real' and the 'estimated' values, mathematically. Most common are sum of squared error (SSE), mean of squared error (MSE), Chi-square-, *t*-, and *F*-tests [27–30].

Each method has advantages and disadvantages and it is not universal to claim which one is the best. SSE, for example, is easy to calculate but is not suitable for the cases, where different sample groups have inconsistent sample sizes [29]. The Chi-square test requires even less computational power and provides detailed statistical information, but is not suitable for a data with large number of categories [31]. Here, we expect different sizes of datasets and chose the MSE as the criterion due to its simplicity and efficiency.

4.2.2 MSE

The MSE is defined as follows [27]:

$$\mathrm{MSE} = \frac{\sum_{i=0}^{N} \left(y\left(x_i\right) - \hat{y}\left(x_i\right)\right)^2}{N} \tag{17}$$

with: N = sample size, $y(x_i)$ = the actual value at ith sample, and $\hat{\boldsymbol{y}}(\boldsymbol{x}_i)$ = the estimated value at ith sample.

As can be seen from Eq. (17), MSE does not require special parameters and is a simple mathematical process. Thus, a low computational cost is expected. Furthermore, according to Wang and Bovik, MSE is 'an excellent metric in the context of optimization' [32]. Due to its convexity, symmetry, and differentiability, iterative numerical optimization is a great use case for MSE, where minimizing the MSE values could play a core role in the optimization process.

4.3 General algorithm

4.3.1 Overview

The developed algorithm to optimize flow curve fitting is a phenomenological approach, as shown in Fig. 10. In addition to the inputs and outputs, the process is characterized by three main parts:

1. initial calibration,
2. individual FEM optimization, and
3. weighted FEM optimization.

In each step, the four hardening models to define a flow curve – Hollomon, Ludwik, Voce, and Swift (see before) – are used. The steps are explained in the following.

The optimization problem for the individual and weighted optimization can be stated as the minimization of MSE as follows:

$$\text{Minimize} \rightarrow \Phi = \mathrm{MSE}\left(s_i, \hat{s}_i\right) \tag{18}$$

Subject to the constraints:

$$\mathrm{Error}_{\varepsilon_{\mathrm{pl,sh}}} \leq \mathrm{Tol}_{\varepsilon_{\mathrm{pl,sh}}} \tag{19}$$

$$\mathrm{Error}_{\sigma_{\mathrm{sh}}} \leq \mathrm{Tol}_{\sigma_{\mathrm{sh}}} \tag{20}$$

$$\mathrm{Error}_{s_u} \leq Tol_{s_u} \tag{21}$$

with: Φ = objective function, $\hat{s}_i$ = engineering stress, simulation, and s_i = engineering stress, experiment.
The tolerances values $\mathrm{Tol}_{\varepsilon_{\mathrm{pl,eL}}}$, $\mathrm{Tol}_{\mathrm{eL}}$, and $\mathrm{Tol}_{\mathrm{s_u}}$ are defined in the inputs and specify allowed tolerances for characteristic points of the stress–strain relationship.

The objective function is limited by the relative error in the mechanical parameters of engineering interest that can be defined from the engineering stress–strain curve and flow curve, as indicated as follows.

4.3.1.1 Strain hardening onset constraint

$$\mathrm{Error}_{\varepsilon_{\mathrm{pl,sh}}} = \left| \frac{\varepsilon_{\mathrm{pl,eL}} - \hat{\varepsilon}_{\mathrm{pl,eL}}}{\varepsilon_{\mathrm{pl,eL}}} \right| \tag{22}$$

with: $\hat{\varepsilon}_{\mathrm{pl,sh}}$ = true plastic strain at the onset of strain hardening, simulation; $\varepsilon_{\mathrm{pl,sh}}$ = true plastic strain at the onset of strain hardening, experiment.

$$\mathrm{Error}_{\sigma_{\mathrm{sh}}} = \left| \frac{\sigma_{\mathrm{sh}} - \hat{\sigma}_{\mathrm{sh}}}{\sigma_{\mathrm{sh}}} \right| \tag{23}$$

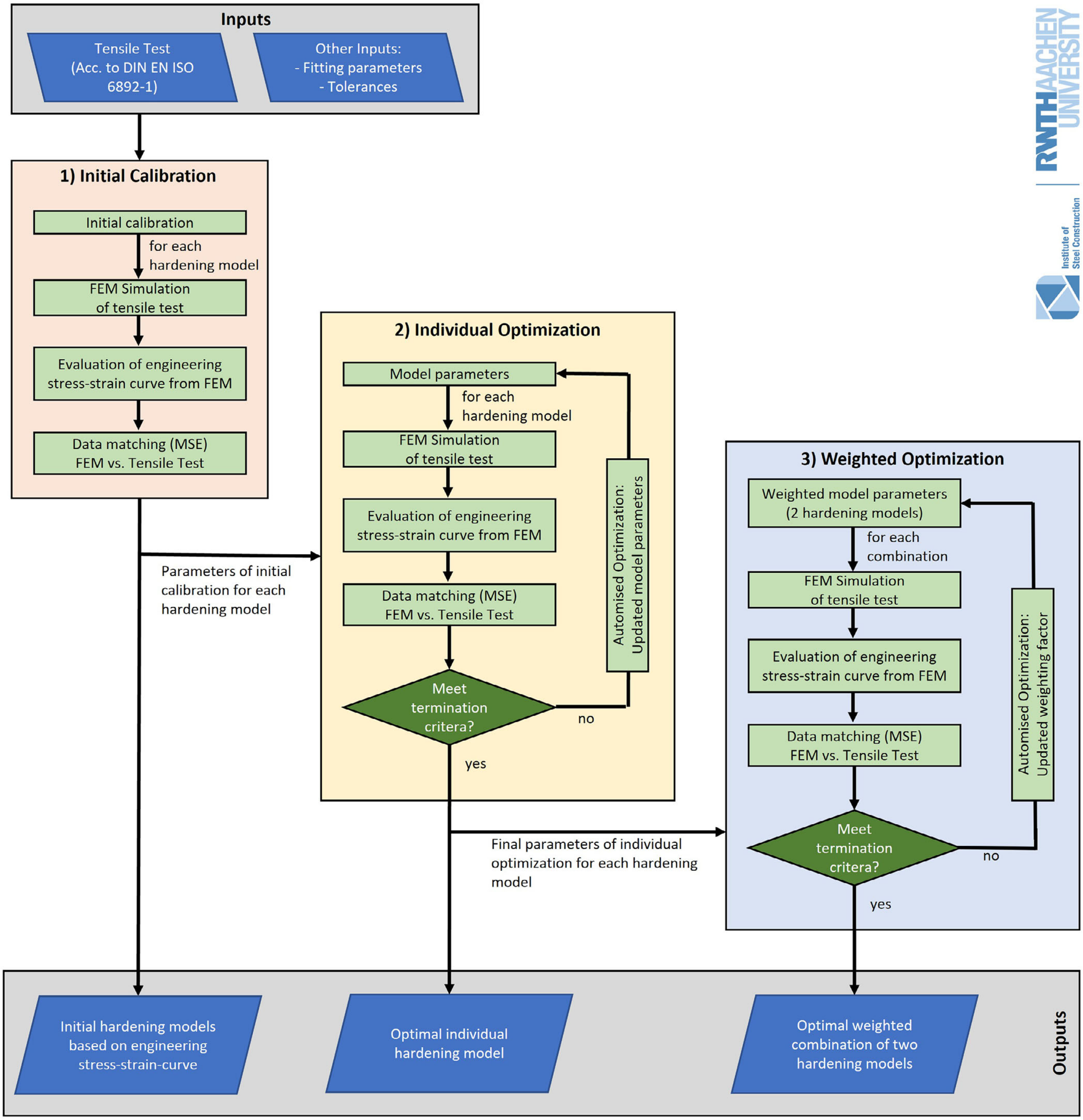

Fig. 10 Flow chart of the developed algorithm to optimize flow curve fitting

with:

$$\sigma_{sh} = \begin{cases} \sigma_y, & \text{for materials without yield plateau} \\ \sigma_{eL}, & \text{for materials with yield plateau} \end{cases}$$

with: $\hat{\sigma}_{sh}$ = true stress at the onset of strain hardening, simulation; $\hat{\sigma}_{sh}$ = true stress at the onset of strain hardening, experiment.

4.3.1.2 Ultimate tensile strength constraint

$$\mathrm{Error}_{s_u} = \left| \frac{s_u - \hat{s}_u}{s_u} \right| \tag{24}$$

with: $\hat{s}_u$ = ultimate tensile strength, simulation; s_u = ultimate tensile strength, experiment.

After the preparation of the inputs, which has to be done manually, the algorithm runs automatically through the steps. The algorithm is implemented to Isight, an optimization software from Dassault Systèmes. Here, all steps are working automatically and the results of the steps were handed over to the specific steps and calculations. Multiple python codes and Isight commands work together, e.g., to automatically create the FEMs for the tensile tests in Abaqus based on the specimen geometry in the input.

4.3.2 Inputs

The inputs can be divided in two types: tensile test inputs and numerical inputs.

4.3.2.1 Tensile test inputs

The tensile test inputs are the main inputs and contain all the data that define the engineering stress–strain curve determined in the tensile test as well as geometric information on the specimen. Here, also all mechanical properties are listed for the initial calibrations of Hollomon and Ludwik model.

4.3.2.2 Other numerical inputs

Other numerical inputs, like the fitting range, in which the data matching is done, or the tolerances for the optimization processes must be defined in advance. These are relevant parameters for the optimization processes.

4.3.3 Data matching evaluation

The data matching is the central aspect in each of the steps of the algorithm. Here, for every new set of parameters for the hardening model, resp. every FE simulation, the resulting engineering stress–strain curve is compared to the experimental engineering stress–strain curve. The data matching algorithm uses MSE to quantify the fit of the simulation to the experiment.

4.3.4 Step 1: Initial calibration

In the first step, the initial calibration, the initial parameters for the hardening models are calculated based on the inputs, especially the mechanical properties based on the tensile test. An FEM is created based on the specimen geometries specified in the inputs. For each hardening model, an FE simulation is done and the results were evaluated with data matching. The initial calibration gives a good overview on which hardening model represents a good first guess and how big the difference is between the tensile test and the FE simulation. The initial flow curve parameters as well as the resulting engineering stress–strain curves are handed over to step 2.

4.3.5 Step 2: Individual optimization

The second step is the individual optimization, where the individual flow curve parameters for each hardening model are getting updated automatically in given limits (defined in the inputs). After each update process, an FE simulation with the updated flow curve is done. Data matching gives a result, if the new parameters have a better fit than the ones before. If the result is within the termination criteria, the optimization for the hardening model is finished. Otherwise, the optimization algorithm decides which parameter will be adjusted in which direction, so that another iteration follows. The results of this step, optimized flow curve parameters for each hardening model, are handed over to step 3.

4.3.6 Step 3: Weighted optimization

In addition to the previous described steps, the weighting sum of two hardening models usually better represents the flow curve [33]. Thus, in the third step, the optimized flow curves for each hardening model act as inputs and two curves get combined with a weighting factor w. The resulting six weighted combinations of flow curves are shown in Tab. 1.

Tab. 1 Weighted hardening models

Combined hardening models	Equation	
Hollomon +Ludwik	$\sigma = w \cdot k_{\mathrm{H}}(\varepsilon_{\mathrm{p}})^{n_{\mathrm{H}}} + (1-w)(\sigma_0 + k_{\mathrm{L}}(\varepsilon_{\mathrm{p}})^{n_{\mathrm{L}}})$	(25)
Hollomon +Voce	$\sigma = w \cdot k_{\mathrm{H}}(\varepsilon_{\mathrm{p}})^{n_{\mathrm{H}}} + (1-w)(\sigma_{\mathrm{sat}} + (\sigma_0 - \sigma_{\mathrm{sat}}) \cdot \exp(-\varepsilon_{\mathrm{p}}/\varepsilon_0))$	(26)
Hollomon +Swift	$\sigma = w \cdot k_{\mathrm{H}}(\varepsilon_{\mathrm{p}})^{n_{\mathrm{H}}} + (1-w)(k_{\mathrm{S}}(\varepsilon_{\mathrm{p}} - \varepsilon_0)^{n_{\mathrm{S}}})$	(27)
Ludwik +Voce	$\sigma = w \cdot (\sigma_0 + k_{\mathrm{L}}(\varepsilon_{\mathrm{p}})^{n_{\mathrm{L}}}) + (1-w)(\sigma_{sat} + (\sigma_0 - \sigma_{sat}) \cdot \exp(-\varepsilon_{\mathrm{p}}/\varepsilon_0))$	(28)
Ludwik +Swift	$\sigma = w \cdot (\sigma_0 + k_{\mathrm{L}}(\varepsilon_{\mathrm{p}})^{n_{\mathrm{L}}}) + (1-w)(k_{\mathrm{S}}(\varepsilon_{\mathrm{p}} - \varepsilon_0)^{n_{\mathrm{S}}})$	(29)
Voce +Swift	$\sigma = w \cdot (\sigma_{\mathrm{sat}} + (\sigma_0 - \sigma_{\mathrm{sat}}) \cdot \exp(-\varepsilon_{\mathrm{p}}/\varepsilon_0)) + (1-w)(k_{\mathrm{S}}(\varepsilon_{\mathrm{p}} - \varepsilon_0)^{n_{S}})$	(30)

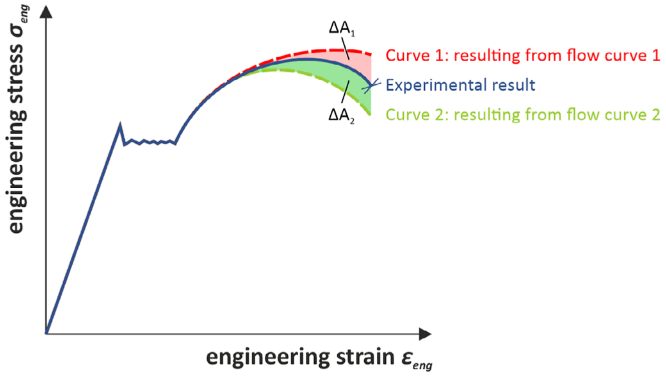

Fig. 11 Schematic depiction of the area differences ΔA_1 and ΔA_2 for two numerically determined stress–strain curves resulting from different flow curves

The parameters for the flow curves are taken from the final result of the individual optimization and are set as fix for this step. Only the weighting factor for each weighted combination is varied iteratively. After each iteration, similar to the individual optimization, a data matching is performed as well as a check if the criteria are fulfilled, which decides whether step 3 is finished or a new iteration is started.

However, some conditions have to be fulfilled to be able to combine the hardening models successfully. Therefore, the weighted optimization requires that: at least two hardening models with engineering stress–strain curves (curve 1 and curve 2) have a positive area difference ΔA_1 and negative area ΔA_2, respectively, to the experimental curve, as shown in Fig. 11.

4.3.7 Output

The outputs of the process contain all the necessary information and parameters to define the hardening models obtained by the initial numerical calibration, individual FEM optimization, and weighted FEM optimization. Also, the resulting engineering stress–strain curves and flow curves are extracted.

5 Numerical validation of the tool

5.1 Mechanical properties of the investigated steels

To evaluate the process and validate the algorithm, a batch of three tensile test results for different high-strength steels made from plates (HSS) was strategically selected. One steel grade, S690QL, has a yield plateau, while the other two, S700MC and pipeline steel X65, have no pronounced yield strength. The fitting range is set for the whole tensile test (until failure strain). The characterization of the main mechanical properties of the investigated steels is shown in Tab. 2.

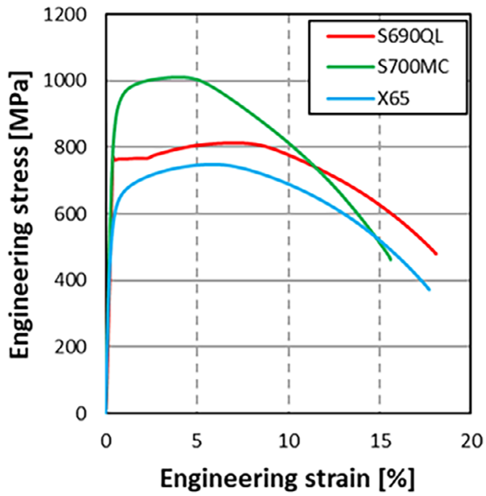

Fig. 12 Engineering stress–strain curves for the investigated steel grades S690QL, S700MC, and X65 based on uniaxial tensile tests (B8x40)

The engineering stress–strain curves extracted from B8x40 tensile tests are shown in Fig. 12.

The inputs have been derived for each steel grade and passed to the fitting tool. The algorithm passed every step based on the procedure shown in Section 4. The results will be discussed in Sections 5.2–5.5. In the end, a validation with component tests is done to demonstrate the transferability from laboratory to component scale, Section 5.6.

5.2 Initial calibration

The initial parameters for each hardening model have been derived based on the result of the tensile test. Parameters as well as the MSE are shown in Tab. 3. Here, also the best fit for each steel grade is indicated.

Tab. 2 Mechanical properties of investigated steels

Steel grade	Specimen type	E [MPa]	f_y [Mpa]	f_{eH} [Mpa]	f_{eL} [Mpa]	f_u [Mpa]	ε_u [%]	Delivery condition
S690QL	B8x40	205682	759	772	770	815	7.06	Quenched and tempered
S700MC	B8x40	234545	896	–	–	1010	4.01	Thermomechanically rolled
X65	B8x40	207832	597	–	–	748	5.91	As-rolled

Tab. 3 Resulting hardening models of the initial calibration for the three steel grades S690QL, S700MC, and X65

Steel grade	Hardening model	Equation	MSE
S690QL	**Hollomon**[a)]	$\boldsymbol{\sigma_H = 1095.3 \cdot (\varepsilon_p)^{0.08}}$	**439**
	Ludwik	$\sigma_L = 789.0 + 879.5 \cdot (\varepsilon_p - 0.02)^{0.74}$	13535
	Swift	$\sigma_{SW} = 1116.7 \cdot (\varepsilon_p - 0.001)^{0.09}$	1081
	Voce	$\sigma_{VC} = 883.4 + (684.1 - 883.4) \cdot \exp(-\varepsilon_p/0.05)$	3663
S700MC	Hollomon	–	–
	Ludwik	$\sigma_L = 899.9 + 1319.2 \cdot (\varepsilon_p)^{0.60}$	78756
	Swift[a)]	$\boldsymbol{\sigma_{SW} = 1251.4 \cdot (\varepsilon_p - 0.001)^{0.05}}$	**2705**
	Voce	$\sigma_{VC} = 1028.9 + (816.7 - 1028.9) \cdot \exp(-\varepsilon_p/0.004)$	5254
X65	Hollomon	–	–
	Ludwik	$\sigma_L = 598.6 + 1047.0 \cdot (\varepsilon_p - 0.02)^{0.55}$	34318
	Swift[a)]	$\boldsymbol{\sigma_{SW} = 1001.3 \cdot (\varepsilon_p - 0.001)^{0.08}}$	**1944**
	Voce	$\sigma_{VC} = 778.4 + (566.4 - 778.4) \cdot \exp(-\varepsilon_p/0.01)$	18563

[a)] Best fit.

The results show that some hardening models represent quite a good fit with the initial calibration, e.g., Hollomon model for S690QL or the Swift model for S700MC, Fig. 13. However, for the steel grades S700MC and X65, the initial calibrations of the hardening models do not fit well. This was also observed in past studies and justifies the development of the flow curve optimization algorithm.

5.3 Individual optimization

In the following, for each hardening model, the optimized individual parameters derived with the algorithm are presented. The range of evaluation and optimum values resulting from this optimization process are summarized in Tab. 4.

With the individual optimization very good results could be achieved, seen by MSE. This proves that by the means of the individual optimized flow curve, a numerical recalculation of the tension test including the necking behaviour is possible, Fig. 14.

5.4 Weighted optimization

In a last step, the weighted optimization was done to improve the fit between numerical and experimental result, Fig. 14. The weighting factors are shown in Tab. 5. With the combined and weighted hardening models, for some steel grades the fit was improved, Tab. 6.

5.5 Summary of the investigations

The final flow curves after every step of the algorithm, as well as the ind/icated best fit, which for the investigated

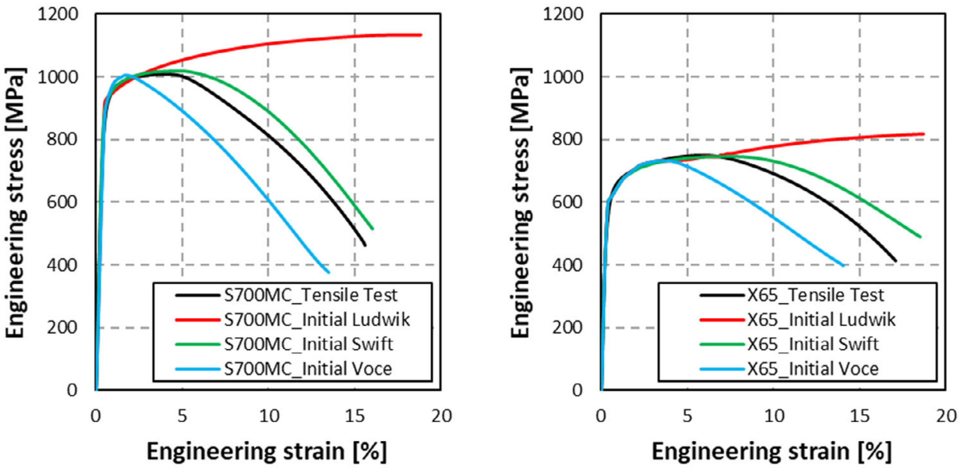

Fig. 13 Comparison between experimental engineering stress–strain curve and the FE results for the initial calibration of the hardening models for S700MC (left) and X65 (right)

Tab. 4 Initial and final values of optimization variable in individual optimization process. Steel grades S690QL, S700MC, and X65

Steel grade	Optimization variable	Min. Value	Max. value	Initial value	Optimized value	Difference optimized/Initial value	MSE
S690QL	Hollomon parameter 1: k_H	1059.4	1119.4	1095.3	**1073.0**	2.1%	225
	Hollomon parameter 2: n_H	0.06	0.1	0.08	**0.0784**	5.1%	
S700MC	Swift parameter 1: k_S	1161.4	1281.4	1251.4	**1209.0**	3.4%	380
	Swift parameter 2: ε_0	0.001	0.007	0.001	**0.003**	195.2%	
	Swift parameter 3: n_S	0.04	0.06	0.05	**0.05**	0.6%	
X65	Swift parameter 1: k_S	881.3	1031.3	1001.3	**950.4**	5.2%	197
	Swift parameter 2: ε_0	0.001	0.009	0.001	**0.001**	0%	
	Swift parameter 3: n_S	0.05	0.09	0.08	**0.07**	13.6%	

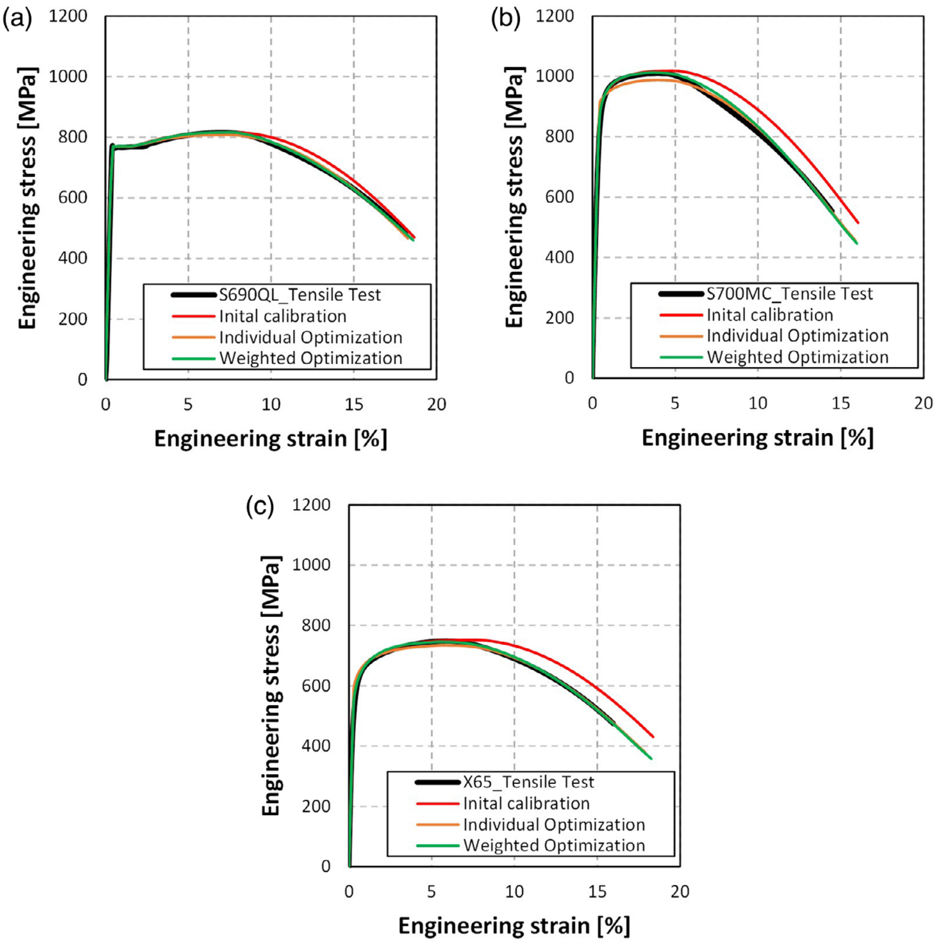

Fig. 14 Comparison of engineering stress–strain curves (best fit for initial calibration, individual, and weighted optimization):a) S690QL, b) S700MC, and c) X65

Tab. 5 Initial and final value of optimization variable in the weighted optimization process for steel grades S690QL, S700MC, and X65

Steel grade	Hardening model	Optimization variable	Min. Value	Max. value	Initial value	Optimized value	Difference optimized/ Initial value
S690QL	Hollomon + Ludwik	weight (w)	0.22	0.36	0.34	**0.264**	25.2%
S700MC	Ludwik + Voce	weight (w)	0.09	0.15	0.09	**0.131**	37.1%
X65	Ludwig + Voce	weight (w)	0.18	0.26	0.24	**0.23**	4.3%

Tab. 6 Final hardening models for steel grades S690QL, S700MC, and X65

Steel grade	Method	Hardening model	Equation	MSE
S690QL	1) Initial calibration	Hollomon model	$\sigma = 1095.3 \cdot (\varepsilon_p)^{0.08}$	439
	2) Individual opt.	Hollomon model	$\sigma = 1073.0 \cdot (\varepsilon_p)^{0.08}$	225
	3) Weighted opt.[a]	**Hollomon + Ludwik model**	$\boldsymbol{\sigma = 0.26 \cdot \sigma_H + 0.74 \cdot \sigma_L}$	**210**
S700MC	1) Initial calibration	Swift model	$\sigma = 1251.4 \cdot (\varepsilon_p - 0.001)^{0.05}$	2705
	2) Individual opt.	Swift model	$\sigma = 1209.0 \cdot (\varepsilon_p - 0.003)^{0.05}$	380
	3) Weighted opt.[a]	**Voce + Swift model**	$\boldsymbol{\sigma = 0.13 \cdot \sigma_{VC} + 0.87 \cdot \sigma_{SW}}$	**255**
X65	1) Initial calibration	Swift model	$\sigma = 1001.3 \cdot (\varepsilon_p - 0.001)^{0.08}$	1944
	2) Individual opt.	Swift model	$\sigma = 950.4 \cdot (\varepsilon_p - 0.001)^{0.07}$	197
	3) Weighted opt.[a]	**Voce + Swift model**	$\boldsymbol{\sigma = 0.23 \cdot \sigma_{VC} + 0.77 \cdot \sigma_{SW}}$	**58**

[a] Best fit.

steels is the weighted optimization, are shown in Tab. 6. The final results for the best fit are shown in Fig. 14.

It can be seen that all four hardening models are represented in the best fit and it is recommendable to implement these. The comparison of the experimentally determined engineering stress–strain curves and the result from the FE simulation with the final flow curve show a very good compliance and the necking behaviour could be modelled correctly. Also, the improvement of the underlying flow curves is very high. It is recommended for future flow curve fittings to use an MSE of around 300 as criterion for a good fit.

5.6 Validation with component tests

To validate the calibrated flow curves, component tests using the materials S690QL and S700MC were evaluated and simulated. The specimens represented lapped splices with M48 bolts of grade 12.9, tested as described in [34]. An example of the test assembly is shown in Fig. 15, where the inner plate is intended to fail. Friction between the plates was excluded using a gap between inner and outer plates, so the force is fully introduced through the bolt.

In the numerical model, the specimen was represented over a defined length, with inductive displacement sensors placed as in the experiment. This ensured that the simulated displacements were directly comparable to the measured values. A refined mesh of 2 mm was applied in the vicinity of the bolt, while a 10 mm mesh was used in the outer regions to ensure computational efficiency. As material input, the weighted optimized flow curves from Tab. 6 were applied. Furthermore, a damage model was implemented to capture specimen failure [34]. This model did not affect the hardening response, which was entirely governed by the flow curves.

Fig. 15 Test setup, specimen LV_1.5 made of S690QL

Fig. 16 presents the comparison for a single-bolted S690QL connection. The simulated force–displacement response aligns closely with the experimental data, with the maximum force deviating by less than 2%. The bearing failure mode observed in the experiment is also reproduced in the simulation.

A similar agreement is obtained for the specimen with two bolts made of S700MC, Fig. 17. Here, the simulated force–displacement behaviour matches the experiment well, and the net-section failure mode is correctly captured. The deviation between the simulated and experimental bearing load is less than 1%.

Additional examples in [34] further confirm the reliability of the fitted flow curves. Overall, the component test validation demonstrates that the calibrated curves provide an accurate basis for numerical simulations.

6 Discussion

With the developed fitting tool, appropriate flow curves, which are mathematically defined, can be derived easily using the developed fitting tool. A validation of experimental tests on laboratory as well as component scale was done and the tests can be modelled realistically with FE methods using the derived flow curves. However, there are limitations and factors to consider when looking at results,

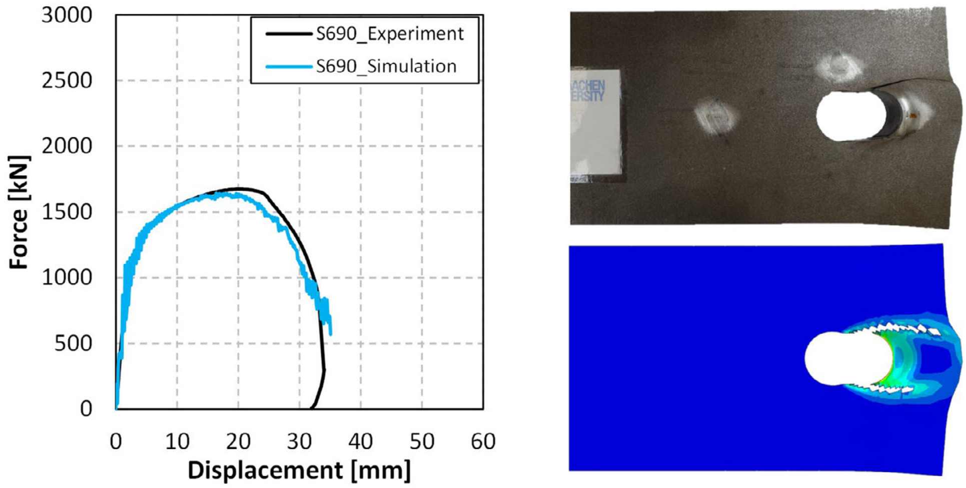

Fig. 16 Comparison of experimental and simulated force–displacement curves (left) and fracture surfaces (right) for specimen LV_1.5 made of S690QL

especially the limitation by the flow curve definition, scattering of tensile tests, and the mesh-size dependency of FE results.

6.1 Limitation by the flow curve definition

The use of the four hardening models limits the range of possible flow curves because of the mathematical definitions. However, the implementation of the third step, the weighted optimization, allows additional flow curves. The results, Section 5, have proven that the use of these four flow curves in addition with the weighted combinations is sufficient and leads to satisfying results.

6.2 Scattering of tensile tests

In general, steel has inhomogeneous material properties, e.g., different behaviour over the thickness of a plate (esp. for thick plates). Also, when tensile tests were conducted, at least three specimens were tested. The results of these three tests may vary, which is why an average engineering stress–strain curve should be chosen as input for the optimization algorithm. Verifications with experiments on component-scale have shown that this is recommendable to predict the component behaviour very well [34].

6.3 Mesh-size dependency

In numerical simulations, the mesh size can have a crucial effect on the result. Therefore, a mesh-sensitivity study has to be done in advance. To exemplarily show the influence of the mesh size, an exemplarily flow curve was applied on a tensile test simulation, B8 × 40 of the S690QL, for different mesh sizes from 0.1 to 2 mm, Fig. 18.

It can be seen that a ‘big’ mesh size compared to the specimen, in this case a mesh size of 2 mm, leads to a change of the resulting yield strength of the specimen as well as a reduced tensile strength. For smaller mesh sizes, the influence on the yield strength and tensile strength

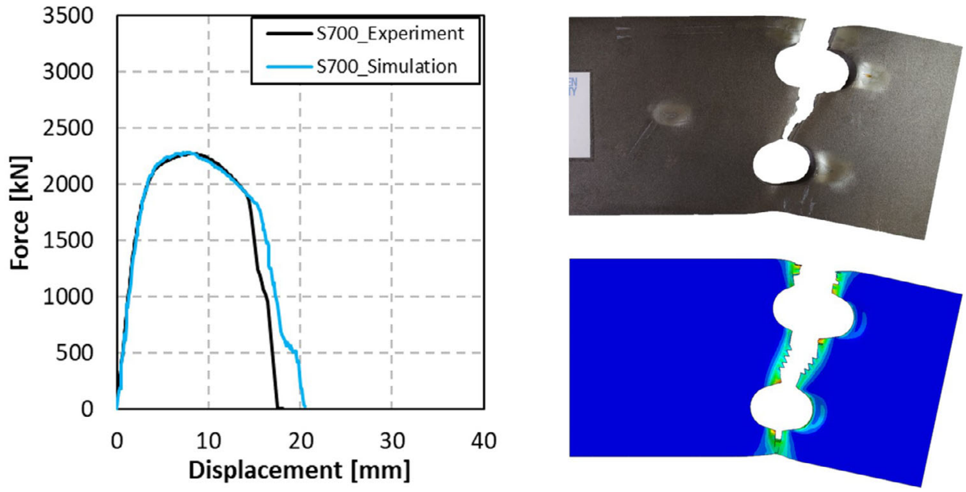

Fig. 17 Comparison of experimental and simulated force–displacement curves (left) and fracture surfaces (right) for specimen LV_2.7 made of S700MC

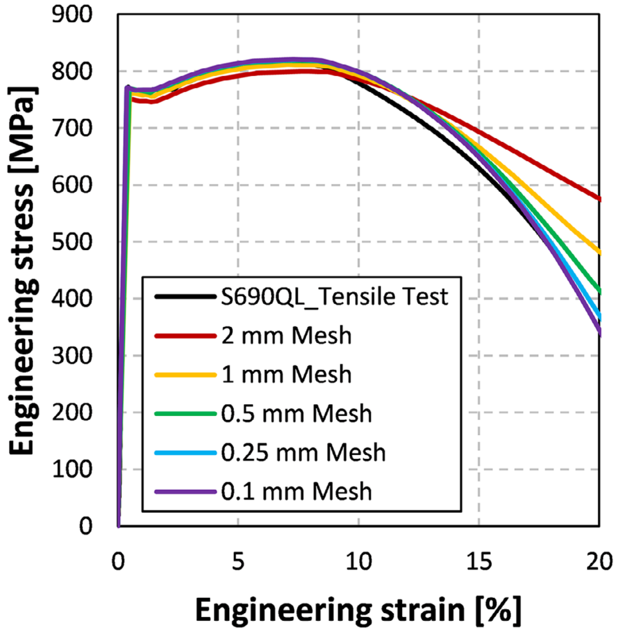

Fig. 18 Influence of the mesh size on the engineering stress–strain curve

is negligible. The necking behaviour is also influenced by the mesh size, which can be seen in the scattering of the curves after reaching the tensile strength. It is important to keep in mind that the final flow curve, after using the tool, is related to the mesh size used in the reference FEM. It is recommended to use a minimum element number of 1 element/1 mm diameter of a round bar.

Considering these effects, powerful flow curves can be derived easily and any stress conditions can be simulated correctly, e.g., [10] or [34].

7 Conclusions and outlook

The following main conclusions are drawn:

1. Utilizing the developed algorithm, flow curves can be systematically derived, enabling realistic numerical modelling of the behaviour of various steels, particularly within the plastic deformation regime, including necking.
2. The algorithm functions autonomously, resulting in considerable time savings and yielding optimized flow curves adhering to mathematical principles.
3. The tool is applicable for different steel grades, including high-strength steels, with and without a yield plateau.
4. The consideration of four different hardening models (Hollomon, Ludwik, Swift, and Voce) as well as the combination of these seems to be reasonable because for the investigated steel grades, different models and combinations lead to the best fit.
5. The flow curves were validated through both laboratory- and component-scale tests and simulations, enabling accurate reproduction of the hardening behaviour across different steel grades.
6. A maximum mean square error of 300 between experimental and numerical result is recommended.
7. A minimum element number of 1 element/1 mm diameter of a round bar is recommended.

The developed tool is used in current research activities [10, 34, 35] in order to prove its power. In this case, the fitting range was set until failure strain, so that the whole necking procedure is implemented in the flow curve. It could be also possible to fit a flow curve only until, e.g., the strain at tensile strength and to overestimate the tensile test afterwards. The necking behaviour could then be simulated by additional use of damage mechanic concepts according to Bai–Wierzbicki or Mohr–Coloumb allowing failure, e.g., cracks, see [34]. Therefore, different sample geometries, such as notched round bars or shear specimens, have to be implemented in the fitting process. Furthermore, additional parameters have to be added to define the damage curves. All in all, the tool could be easily adapted for different geometries. With its use, the forecast quality of numerical simulations can be improved drastically. In the future, calibrated numerical models will be used even more to, e.g., develop design guidelines for different challenges in steel construction.

Acknowledgements

The tool was developed within the IGF project 'Innovative load-bearing capacity analysis of welded steel components using damage mechanics', IGF project no. 20875 N, of the Forschungsvereinigung Stahlanwendung e. V. (FOSTA), Sohnstraße 65, 40237 Düsseldorf. It was funded via the AiF within the framework of the programme for the promotion of joint industrial research (IGF) by the Federal Ministry of Economics and Climate Protection on the basis of a resolution of the German Bundestag.

Open access funding enabled and organized by Projekt DEAL.

References

[1] Bartsch, H. et al. (2021) *Experimental and numerical investigations on the rotation capacity of high-strength steel beams*. Journal of Structural Engineering 4, pp. 1630–1636.

[2] Bartsch, H.; Eyben, F.; Schaffrath, S.; Feldmann, M. (2021) *On the plastic design of high-strength steel beams*. Steel Construction 14, pp. 225–235.

[3] Brinnel, V.; Schaffrath, S.; Münstermann, S.; Feldmann, M. (2016) *Validation of a concept for burst pressure prediction by damage mechanics*. ASME 2016 Pressure Vessels and Piping Conference 6A: Materials and Fabrication, https://doi.org/10.1115/PVP2016-63236

[4] Schillo, N. et al. (2016) *Rules on high strength steel (RUOSTE) – Final Report*. Brussels: European Commission.

[5] Bartsch, H. et al. (2020) *Damage mechanics based failure prediction for structures under seismic action*. Journal of Constructional Steel Research 173, p. 106264.

[6] prEN 1993-1-14 (2023) *Eurocode 3 – Design of steel structures – Part 1–14: Design assisted by finite element analysis*.

[7] Hollomon, J. H. (1945) *Tensile deformation*. Transactions of the AIME 162, pp. 268–290.

[8] Ludwig, P. (1909) *Elemente der Technologischen Mechanik*. Berlin: Springer.

[9] Ramberg, W.; Osgood, W. R. (1943) *Description of stress–strain curves by three parameters*. NASA Scientific and Technical Information Facility – NACA-TN-902 (Technical Note No. 902).

[10] Eyben, F. et al. (2023) *Innovative Tragähigkeitsanalyse geschweißter Stahlbauteile mit Hilfe der Schädigungsmechanik (Schlussbericht Fosta-P1415)*. Düsseldorf: Verlag und Vertriebsgesellschaft mbH.

[11] DIN EN ISO 6892-1 (2019) *Tensile testing – Part 1: Method of test at room temperature*.

[12] DIN 50125 (2021) *Prüfung metallischer Werkstoffe – Zugproben*.

[13] Bhaduri, A. (2018) *Mechanical properties and working of metals and alloys*. Singapore: Springer.

[14] Roylance, D. (2001) *Stress-Strain Curves*. Cambridge, MA: Department of Materials Science and Engineering, Massachusetts Institute of Technology.

[15] Davis, J. (2004) *Tensile testing*. Ohio, USA: ASM International.

[16] M. S. Engineering, *True stress-strain vs. engineering stress-strain* [Online]. https://msestudent.com/true-stress-strain-vs-engineering-stress-strain/ [accessed on: 12 Sep. 2023]

[17] Slater, R. (1977) *Engineering plasticity: Theory and application to metal forming processes*. London: Department of Mechanical Engineering.

[18] Kopp, R.; Wiegels, H. (1999) *Einführung in die Umformtechnik*, 2. korrigierte Auflage. Aachen: Verlag Günter Mainz.

[19] FormingWorld, *Material Matters: Sheet metal plasticity visualized (part 2 of 2)* [Online]. https://formingworld.com/sheet-metal-plasticity-visualized-part-2-of-2/ [accessed on: 12 Sep. 2023]

[20] Hering, O.; Kolpak, F.; Tekkaya, A. E. (2019) *Flow curves up to high strains considering load reversal and damage*. International Journal of Material Forming 12.

[21] Tu, S.; Ren, X.; He, J.; Zhang, Z. (2020) *Stress-strain curves of metallic materials and post-necking strain hardening characterization: A review*. Fatigue and Fracture of Engineering Materials and Structures 1, pp. 3–19.

[22] Zhuang, X.; Zhao, Z.; Li, H.; Xiang, H. (2013) *Experimental methodology for obtaining the flow curve of sheet materials in a wide range of strains*. Steel Research International 84, pp. 146–154.

[23] Samuel, K. G. (2006) *Limitations of Hollomon and Ludwigson stress–strain relations in assessing the strain hardening parameters*. Journal of Physics D: Applied Physics 39, pp. 203–212.

[24] Swift, H. (1952) *Plastic instability under plane stress*. Journal of the Mechanics and Physics of Solids 1, pp. 1–18.

[25] Voce, E. (1948) *The relationship between stress and strain for homogenous deformations*. Journal of the Institute of Metals 74, pp. 537–562.

[26] Sadowski, A. J. et al. (2017) *On the gradient of the yield plateau in structural carbon steels*. Journal of Constructional Steel Research 130, pp. 120–130.

[27] Dekking, F.; Kraaikamp, C.; Lopuhaä, H.; Meester, L. (2005) *Modern Introduction to Probability and Statistics. Understanding Why and How*. London: Springer.

[28] Rohatgi, V. K.; Saleh, M. E. A. K. (2015) *An introduction to probability and statistics* (3rd ed.). Hoboken, NJ.

[29] Pestman, W. (2009) *Mathematical statistics*. Berlin: de Gruyter.

[30] Ross, S. (2017) *Chi-squared goodness-of-fit tests in: Introductory statistics*.

[31] McHugh, M. (2029) *The chi-square test of independence*. Biochemical Medicine, 23, pp. 143–149.

[32] Wang, Z.; Bovik, A. C. (2009) *Mean squared error: Love it or leave it? A new look at Signal Fidelity Measures*. IEEE Signal Processing Magazine 26, pp. 98–117.

[33] Defaisse, C.; Mazière, M.; Marcin, L.; Besson, J. (2018) *Ductile fracture of an ultra-high strength steel under low to moderate stress triaxiality*. Engineering Fracture Mechanics, 194, pp. 301–318.

[34] Eyben, F. et al. *(2024, under review) Optimierung freier Stahlbaugeometrien unter beliebigen Beanspruchungszuständen mit Hilfe der Schädigungsmechanik (Schlussbericht Fosta-P1458)*. Verlag und Vertriebsgesellschaft mbH (Düsseldorf, Germany).

[35] Feldmann, M. et al. (2023) *Stand der Untersuchungen zu Werkstoffanforderungen hochfester Stähle S700 bis S960 – FOSTA-Forschungsverbund HOCHFEST*. Stahlbau 92, No. 8, pp. 468–483.

Authors

Felix Eyben (corresponding author)
f.eyben@stb.rwth-aachen.de
RWTH Aachen University
Institute of Steel Construction
Mies-van-der-Rohe Straße 1
52066 Aachen
Germany

Dr.-Ing. Helen Bartsch
h.bartsch@stb.rwth-aachen.de
RWTH Aachen University
Institute of Steel Construction
Mies-van-der-Rohe Straße 1
52066 Aachen
Germany

Prof. Dr.-Ing. Markus Feldmann
feldmann@stb.rwth-aachen.de
RWTH Aachen University
Institute of Steel Construction
Mies-van-der-Rohe Straße 1
52066 Aachen
Germany

How to Cite this Paper

Eyben, F.; Bartsch, H.; Feldmann, M. (2026) *Fitting of mechanical material behaviour of structural steel for numerical modelling: Development of an optimization algorithm*. Steel Construction, P. 1–16.
https://doi.org/10.1002/stco.70013

This paper has been peer reviewed. Submitted: 1 December 2025; accepted: 6 January 2026.